Crystallization in acidic media: from nanoparticles to macrocrystals

/ Javier Sanchez España

Instituto Geológico y Minero de España, Calera, 1, 28760, Tres Cantos, Madrid, Spain. j.sanchez@igme.es

Abstract

Crystallization in acidic media obeys the same rules and physico-chemical principles than in any other aqueous solution. However, the composition (mineralogy), particle size and crystallinity of the solids formed in these low pH systems are strongly determined by (i) the singular water chemistry of the parent acidic solutions (highly concentrated, with presence of many dissolved metals, and usually dominated by the sulfate anion, SO_4^{2-}), and (ii) the highly variable environmental conditions prevailing in the crystallization media (which may range from very fast to slow precipitation kinetics, from strong oversaturation to near solubility equilibrium, or from high to low density of nucleation centres). The most common mineral groups formed in acidic waters (e.g., acid mine waters, acid rock drainage) are usually metal sulfates, oxy-hydroxysulfates and sulfides, which expand largely in size (from nano-particles with diameters < 100 nm to large crystals of mm- to cm-scale) and crystalline order (nearly amorphous or short-range ordered to highly crystalline).

Key-words: *sulfates, sulfides, nanoparticles, crystal growth, kinetics, mineral solubility, acidic waters*

1. Introduction

Crystallization is commonly defined as the process (natural or artificial) by which a solid is formed after atom or molecule organization in a well-defined structure known as a crystal *(Mullin, 2001)*. In the majority of cases, this process takes place in an aqueous solution through precipitation at low (ambient) temperature, though it may also take place from a melt or from a gas at higher temperatures. Crystallization and precipitation are therefore closely related concepts. The difference between them is that in the former case the product is always ordered (the crystal), while in the later, the solid may also be amorphous or disordered.

Crystallization in acidic media obeys exactly the same rules and identical physical and chemical principles than in any other aqueous solution. However, the particular nature and chemical features of *natural* acidic waters imposes certain restrictions and general trends which affect to a great extent the crystallinity (=degree of structural order within the crystal) and size of the formed solids in these solutions. Here, the term *"natural"* refers to the fact that acidic solutions form spontaneously as a result of natural chemical reactions (e.g., pyrite oxidation), even if such reactions occur in deeply anthropogenic and severely man-modified environments, such as mining operations or waste disposal sites.

In addition to the parameter which most obviously defines these waters (i.e., high acidity, low pH), the singular water chemistry of what is commonly referred to as *acid mine drainage* (AMD) or *acidic mine waters*, includes characteristics such as (i) very high solute concentrations and ionic strengths which largely exceed those usually encountered in dilute solutions and fresh waters, (ii) presence of many dissolved metals (e.g., Fe, Al, Cu, Zn, Mn) and metalloids (e.g., As), resulting from the dissolution of different reacti-

ve minerals, and (iii) omnipresence of the sulfate anion (SO_4^{2-}), as a natural consequence of sulphide (mostly pyrite) dissolution, and which determines the ionic complexes forming in the solutions (metal-sulfate complexes) and the mineralogical nature of the solids formed, dominated by sulfates, oxy-hydroxysulfates and/or secondary sulfides, depending on the pH and redox conditions *(Nordstrom & Alpers, 1999a)*.

The environmental conditions prevailing in the crystallization media may also be highly variable (e.g., totally anaerobic and highly reducing to fully oxygenated and oxidising, running waters with turbulent flow to standing waters with laminar or negligible flow, abundance or scarcity of microorganisms, etc...), thus leading to notably different crystallization patterns and resulting mineral products. This variability affects to critical aspects such as (i) precipitation kinetics (from very fast to slow), (ii) saturation state (from strong oversaturation to near solubility equilibrium), or (iii) abundance or scarcity of nucleation centres (high to low density).

In this review, I firstly provide some brief fundamentals on crystallization and acid mine water chemistry, and then I describe the most important solids (nearly amorphous or short-ranged ordered to highly crystalline) forming in acidic waters, along with the chemical conditions leading to their formation (precipitation or crystallization), and the main mineralogical characteristics of these solids. For simplicity, these solids are grouped by mineral types and chemical environments.

2. General concepts of crystallization

The process of crystallization consists of two major stages, *nucleation and crystal growth*. These two stages are both controlled by well-known thermodynamic and kinetic principles. In nucleation, the solutes (atoms, molecules) originally dispersed in the solution start to group into clusters which increase the solute concentration in micro-scale regions. These regions of higher solute density and cluster rearrangement are called the *nuclei*. Crystal growth is the stage by which nuclei that reach a *critical size* (which is controlled by temperature or supersaturation) become larger in size due to farther atom or molecule incorporation. The arrangement of atoms around the nuclei takes place in a periodic and well-defined manner, which defines the *crystal structure (Ashcroft & Mermin, 1976)*.

Crystal growth is essentially a dynamic process and usually occurs under equilibrium conditions, where atoms or molecules precipitate out of solution or dissolve back into solution depending on the solubility (K_{sp}) of the species involved. Depending on the conditions in the crystallization medium, nucleation may predominate over crystal growth, or crystal growth may predominate over nucleation, and this balance dictates crystal size (more abundant crystals of smaller size in the former case, and fewer crystals of larger size in the latter). Nucleation and crystal growth are both under kinetic, more than thermodynamic, control.

2.1. Nucleation

Nucleation may be *homogeneous or heterogeneous* depending on whether it takes places directly from the solution without the participation of any solid surface or, on the other hand, it occurs with the mediation of solid surfaces which catalyse and make the process possible *(e.g., Yang & Qiu, 1986)*. Purely homogeneous nucleation is a highly energy-demanding process (requires an important amount of activation energy), and rarely occurs in nature. Thus, nucleation is commonly heterogeneous and catalysed by any pre-existing solid surfaces, which may comprise from colloidal or dust particles to bacterial cells.

In another classification (somehow comparable to the former), nucleation is also commonly divided into *primary and secondary* nucleation, with the former comprising the early stages of nucleation taking place in the solution with no presence of crystals or solids, and the later involving the subsequent stages of crystal for-

 Depósito legal: CA-602-2004 / ISSN: 1698-5478

mation with an important influence of the formed crystals, which would act as *seeds* favouring and catalysing the formation of more nuclei in the interface between the solution and the crystal surfaces.

The nucleation rate is usually defined by the following equation (*Tavare, 1995*):

$$B = [dN/dt] = k_n (c\text{-}c^*)^n \qquad (1)$$

Where B is the number of nuclei formed per unit volume and unit time, N is the number of nuclei per unit volume, K_n is the rate constant, c is the solution concentration in a given time, c* is the solution concentration at saturation, and n is an empirical exponent which usually ranges between 3 and 4. The term (c-c*) is usually known as the supersaturation value, and basically defines the quantity of solute available for the growth of the crystal.

2.2. Saturation and precipitation kinetics

Supersaturation is a major driving force of crystallization in aqueous media. The degree of saturation of a given solution with respect to the solubility of a certain solid is usually defined as the saturation index, SI, by the expression:

$$SI = \text{Log } [IAP/K_{sp}] \qquad (2)$$

Where, IAP is the ionic activity product, and K_{sp} is the solubility product constant of the solid. Under equilibrium conditions, SI approaches zero (SI=0). When the concentration of solutes forming a given mineral phase is well below a critical value (the solubility product constant, K_{sp}), SI is negative and indicates that no nucleation or crystallization of that mineral will take place. On the other hand, when the solute concentration reaches the critical solubility limit, then SI becomes positive and the mineral may start precipitating out of solution. The higher the SI value, the more supersaturated is the solution, and the more thermodynamically favourable is the precipitation of that mineral.

Although there is not a direct relation between SI and the kinetics of the precipitation process, as discussed below, the near-zero SI values indicating solubility equilibrium are usually associated with slow precipitation and crystallization kinetics (also with low nucleation rates, B), where the physical conditions (i.e., crystallization predominating over nucleation) favour the formation of fewer but larger and highly-ordered, crystalline solids. On the other hand, when a high chemical (e.g., pH, redox) disequilibrium occurs in the solution, the saturation indices may become abruptly very high as a natural response to quickly changing physico-chemical conditions. Under these circumstances, B (in equation 1) may be higher, nucleation and precipitation kinetics faster, nucleation predominates over crystallization (more abundant nuclei) and the resulting solids usually show lower crystal size (diameter) and crystalline order. Examples of the first situation related to acidic mine waters include evaporative pools with concentrated brines or porewaters within sediments, with no or negligible motion, and in which solute concentration eventually reaches the solubility limit, so that macroscopic crystals start forming and develop in the bulk solution or in interstitial space between soil or sediment particles. Examples for the second situation include anoxic waters emerging from mine portals or seeping from taillings or waste piles, and which suddenly get in contact with atmospheric O_2 which oxidizes reduced substances and provoke the appearance of oxidized species with much lower solubility compared to their reduced counterparts (e.g., Fe^{3+} as compared to Fe^{2+}), or mixing zones between acidic effluents and pristine water courses which provoke sharp pH gradients in spatially very restricted areas (e.g., often in a cm- or mm-scale). These environments are usually associated with low particle sizes and low degrees of crystalline order.

3. Chemistry of typical acid mine drainage solutions

Apart from being one of the most important (and most extensively studied) chemical reactions occurring in nature, the oxidation of pyrite is also responsible for the

formation of acidic mine drainage (Singer & Stumm, 1970; Nordstrom & Alpers, 1999a). The oxidation of pyrite in the presence of oxygen and water is chemically described by the reaction:

$$FeS_{2(s)} + 3.5\ O_2 + H_2O \rightarrow Fe^{2+} + 2\ SO_4^{2-} + 2\ H^+ \qquad (3)$$

A very important chemical reaction associated with pyrite oxidation is the subsequent oxidation of the ferrous iron released in reaction (3), which is defined by reaction (4):

$$14\ Fe^{2+} + 3.5\ O_2 + 14\ H^+ \rightarrow 14\ Fe^{3+} + 7\ H_2O \qquad (4)$$

In the absence of molecular oxygen, ferric iron (Fe^{3+}) can also oxidize pyrite through reaction (5):

$$FeS_{2(s)} + 14\ Fe^{3+} + 8\ H_2O \rightarrow 15\ Fe^{2+} + 2\ SO_4^{2-} + 16\ H^+ \qquad (5)$$

This second oxidation pathway is, in fact, much faster than the oxygen pathway *(Garrels & Thompson, 1960; McKibben & Barnes, 1986)*.

Under acidic conditions (e.g., pH<3.5), reaction (4) is much slower than reaction (3), so that the oxidation of Fe^{2+} by oxygen is considered the *rate-limiting step (Singer & Stumm, 1970)*. The presence of acidophilic bacteria, however, accelerates the oxidation rate by a factor of ~10^6 with respect with the abiotic rate *(Singer & Stumm, 1970*; *Nordstrom & Alpers, 1999a)*. Thus, microorganisms play a critical role in pyrite oxidation and AMD generation by maintaining a high concentration of ferric iron in the system. Oxygen will always be required to replenish the supply of ferric iron according to reaction (4), so that the overall rate of pyrite oxidation in a tailings or waste pile or in an underground mine will largely depend on the overall rate of oxygen transport by advection and diffusion *(Nordstrom & Alpers, 1999a; Ritchie, 2003)*.

The stoichiometry of reaction (3) shows that the oxidation of pyrite inevitably leads to acidic solutions with dissolved iron and sulfate as major solutes. The concentration of acidity (protons, H^+), iron and sulfate in the solutions, as well as the redox state of iron (ferrous vs. ferric) will depend on many different factors, including: (i) residence time of the water body (e.g., aquifer) or stream (e.g., effluent) within the mine or waste (=reaction time), (ii) [rock/water] ratio, (iii) pyrite content within the rock matrix, (iv) grain size (the smaller the more reactive), (v) concentration and metabolic activity of acidophilic, iron-oxidising bacteria in the mine sites, or (vi) temperature (which affects the bacterial metabolism to a great extent), to name only a few. Many acidic mine waters around the world may exhibit sulfate and iron concentrations in the order of hundreds of mg/L and up to tens or even hundreds of grams per liter (g/L) in the most extreme cases (e.g., *Nordstrom & Alpers, 1999b; Alpers et al., 2003; Sánchez-España et al., 2008*). In addition, the low pH of these acidic waters provokes the dissolution of reactive minerals present in the host rocks, such as other sulfides (e.g., sphalerite, chalcopyrite, arsenopyrite, galena), carbonates (e.g., calcite, siderite) or aluminosilicates (e.g., feldspar, chlorite, illite/muscovite). Therefore, AMD waters usually include very high concentrations of many others metals (e.g., Al, Mn, Cu, Zn, Co, Ni, Cd) and metalloids (e.g., As), in addition to other alkaline and alkaline earth metal cations (e.g., Mg, Ca, Na, K).

The redox chemistry of AMD is mostly controlled by the iron redox chemistry, which is in turn controlled by the availability of O_2, as discussed before (reaction 4). In deep underground mines or within tailings and waste piles, the rate of oxygen consumption largely exceeds the replenishment of O_2 through advection and diffusion, and waters are usually anoxic (i.e., devoid of oxygen), so that ferrous iron stays reduced in a large proportion. On the other hand,

at near-surface conditions, O_2 is more readily available (it is not a limiting reactant), and iron is oxidized at rates commonly typical of bacterial mediation *(Nordstrom, 1985; Sánchez-España et al., 2007a)*.

4. Oxy-hydroxysulfate nanoparticles resulting from Fe(III) and Al precipitation

The conventional assumption defines nanoparticles as those having sizes comprised between 1 and 100 nm (e.g., *Hochella, 2008*). The biogeochemical conditions of acid mine waters favor the precipitation of certain mineral phases which tend to form particles with sizes close to this limit of particle size, and therefore can be considered as nanoparticles. These nm-sized particles may later coalesce and form mineral aggregates of larger (e.g., sub-micron) size, but when observed under SEM or TEM, it is often possible to identify the original nanometric units forming those aggregates. Their small size makes them behave as colloids in the solutions (i.e., they do not settle and their physical transport may be comparable to that of solutes). This small size also confers these particles a very high specific surface area and a very high sorbent capacity, which make these phases an important element in the transport of many contaminants (heavy metals and metalloids) and critical nutrients (e.g., phosphate, organic compounds). The two most classical and important examples are those of schwertmannite (an Fe(III)-oxyhydroxysulfate resulting from ferric iron precipitation at pH 2.5-4.0) and hydrobasaluminite (an Al-bearing oxyhydroxysulfate formed by Al^{3+} precipitation at pH>4.0). These two minerals have very low crystallinity, though they are not amorphous at all. Instead of well-defined, narrow peaks, their XRD patterns show broad reflections diagnostic of short-range order *(Bigham et al., 1996; Bigham & Nordstrom, 2000; Sánchez-España, 2007; Sánchez-España et al., 2011)*.

4.1. Schwertmannite and its transformation to jarosite crystals

The solid formed by precipitation of $Fe^{(III)}$ in AMD solutions at pH 2.5-3.5 is usually schwertmannite *(Bigham et al., 1994, 1996; Bigham & Nordstrom, 2000, Kawano & Tomtita, 2001)*. The precipitation of schwertmannite is given by the reaction:

$$8\ Fe^{3+} + SO_4^{=} + 14\ H_2O \Leftrightarrow Fe_8O_8(SO_4)(OH)_6 + 22H^+ \quad (6)$$

The crystal system of this mineral is tetragonal-dipyramidal (P 4/m), with an akaganéite-like structure, Fe^{3+} atoms in octahedral coordination and bridging complexes between Fe and SO_4 *(Singer & Stumm, 1970)*. Under experimental conditions (e.g., during titration with fast precipitation rate) it may form pseudo-spherical particles with diameters around 100 nm *(Fig. 1a)*, though its more typical morphology is usually that of hedgehog (or pin-cushion), which is composed of nanometric needles or whiskers with thickness <4-5 nm and lengths of 50-100 nm *(Fig. 1b-d) (Bigham et al., 1994, 1996; Sánchez-España et al., 2011, 2012, 2016a)*.

The occurrence of schwertmannite is closely associated with the presence of iron-oxidising, acidophilic bacteria, which are needed to oxidize Fe(II) to Fe(III) at low pH, as discussed previously. For this reason, the acicular, needle-like morphology of this mineral has been sometimes interpreted to result from biomineralization or mineral encrustation of rod-like bacterial cells *(e.g., Ferris et al., 2004)*. However, different laboratory studies have shown that the presence of bacteria is not actually needed, and hedgehog schwertmannite may also form under purely abiotic conditions *(e.g., Goetz et al., 2010)*. The needles forming the structure of schwertmannite particles are more likely the result of preferential mineral growth along a specific direction, and seems to be kinetically (not biotically) controlled.

An important aspect about the geochemistry of schwertmannite is that, although its formation is kinetically favored with respect to other iron-bearing phases and this mineral is usually

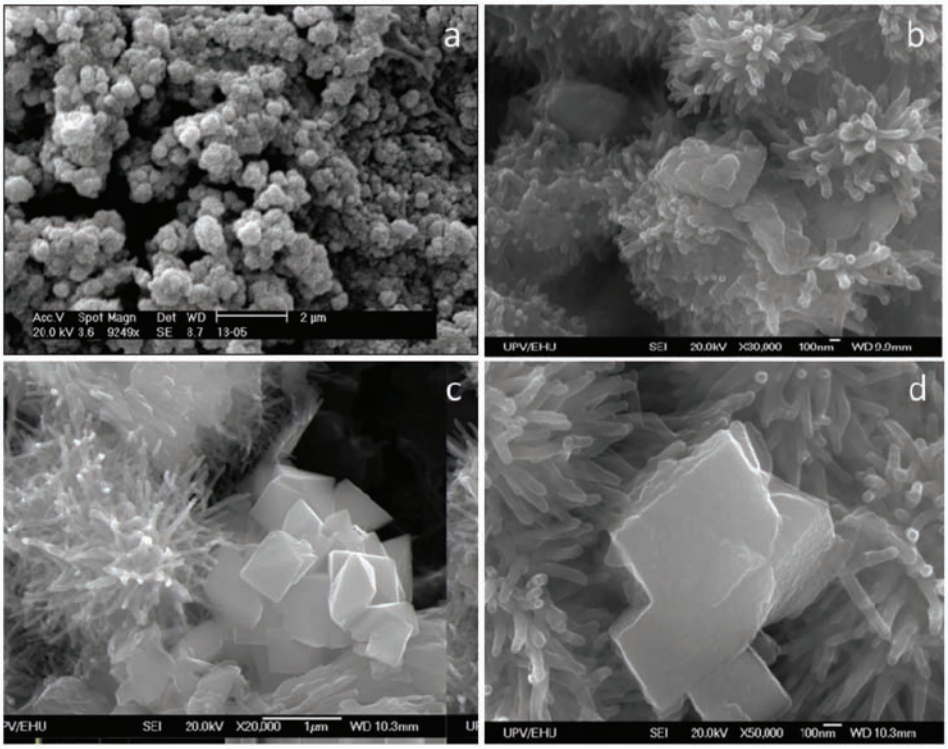

Fig. 1. Schwertmannite particles formed by ferric iron precipitation in acidic waters at pH 2.5-3.5: (a) globular schwertmannite particles formed in the lab during titration of acidic solutions with NaOH 1 M; (b-d) natural schwertmannite particles found in the acidic pit lake of San Telmo (Huelva, Spain) showing characteristic hedgehog morphology, and coexisting with euhedral crystals of jarosite. Compiled from Sánchez-España et al., 2011, 2012, with permission.

the first product of Fe(III) precipitation in the pH window of 2.5-4.0, it is metastable and tends to transform to other mineral phases such as jarosite or goethite, depending on the hydrochemical conditions (pH, pe, SO_4 concentration, etc.) *(Bigham et al., 1996; Bigham & Nordstrom, 2000; Sánchez-España et al., 2011)*. Under low pH (e.g., <2.5-3.0) and high sulfate concentrations (~0.1 M SO_4^{2-}), jarosite is usually the more stable ferric iron mineral. The mineral transformation of schwertmannite to jarosite may take place in the sediments of acidic streams and lakes *(e.g., Regenspurg et al., 2004; Acero et al., 2006; Jönsson et al., 2005)* or directly in the water column of lakes or acidic reservoirs *(e.g.; Sánchez-España et al., 2011, 2012) (Fig. 1c-d)*. Thus, it is rather common to observe hedgehog schwertmannite coexisting with euhedral crystals of jarosite which have been formed by transformation of the former *(Fig. 1c-d)*. Jarosite formed in these acidic environments can be variable in composition (e.g., from potassium jarosite to hydronian jarosite), though the most common case is that of a solid solution with variable amounts of K+ and H_3O^+ in the alkali site *(Alpers et al., 1989; Dutrizac & Jambor, 2000; Stoffregen et al., 2000; Sánchez-España et al., 2012)*. Thus, the conversion of schwertmannite to jarosite can be represented by the reaction:

$$Fe_8O_8SO_4(OH)_6{\cdot}10H_2O_{(s)} + 0.5K^+_{(aq)} + SO_4^{2-}{}_{(aq)} + 16.5H^+_{(aq)} \rightarrow (H_3O_{0.50}K_{0.50})Fe_3(SO_4)^2(OH)_{6\ (s)} + 5Fe^{3+}_{(aq)} + 18.5H_2O_{(l)} \quad (7)$$

This transformation may comprise different stages of dissolution and reprecipitation in a manner that it is often possible to observe newly formed jarosite crystals with remnant schwertmannite wiskers which still have not been replaced *(Fig. 2)*.

Depósito legal: CA-602-2004 / ISSN: 1698-5478

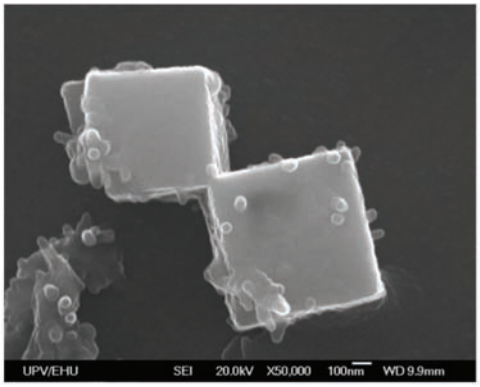

Fig. 2. Pseudocubic crystals of jarosite formed in San Telmo acidic pit lake (Huelva, Spain) after transformation of former schwertmannite needles, some of which can still be observed. Reprinted from Sánchez-España et al., (2012) with permission from The Mineralogical Society of Great Britain and Northern Ireland.

4.2. Hydrobasaluminite and its transformation to Al oxides and/or aluminosilicates

Another process which also leads to submicron- to nanoparticle formation in acidic systems is the precipitation of aluminum. In fresh dilute waters this process usually takes place at pH around 5.0, when Al flocs (typically consisting in gibbsite or amorphous $Al(OH)_3$) precipitate out of solution *(Nordstrom & Ball, 1986; Furrer et al., 2002)*. In solutions with high sulfate concentration (e.g., AMD), however, this process takes place at comparatively lower pH (around 4.0-4.5) and the solid formed is usually a nearly amorphous oxyhydroxysulfate with stoichiometry between hydrobasaluminite and felsöbanyaite *(Nodstrom, 1982; Bigham & Nordstrom, 2000; Sánchez-España, 2007; Sánchez-España et al., 2006, 2011, 2016b)*. The hydrolysis of Al^{3+} to form hydrobasaluminite is described as follows:

$$4\ Al^{3+} + SO_4^{=} + 22\text{-}46\ H_2O \Leftrightarrow Al_4(SO_4)(OH)_{10}\cdot 12\text{-}36H_2O + 10\ H^{+} \quad (8)$$

The size and morphology of the hydrobasaluminite particles formed by reaction (8) largely depends on precipitation kinetics, which may in turn vary from fast precipitation rates in mixing zones with very sharp pH gradients leading to oversaturation, to slow rates in near-equilibrium or slightly saturated systems (e.g., water column of acidic lakes). Under SEM, most particles are pseudo-spherical and around 1 mm in diameter *(Fig. 3a)*, and the XRD analyses can only detect two broad reflections near 7 and 20 º2θ *(Fig. 3b)*.

However, detailed investigations by TEM have revealed that the diameter of some hydrobasaluminite particles can be much smaller (as low as 100-200 nm) and may even show certain crystal faces indicative of partial recrystallization *(Fig. 4a)*. Further, hydrobasaluminite is known to be metastable with respect to other Al phases, such as oxides (e.g., gibbsite, bayerite) or aluminosilicates (e.g., allophane), so that nanometer-scale crystals of the latter minerals can be observed in the sponge-like amorphous matrix of the

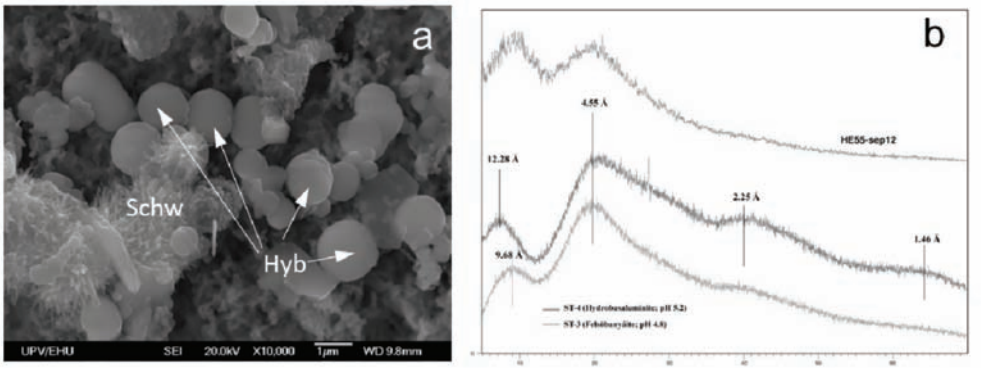

Fig. 3. a) SEM picture of hydrobasaluminite (Hyb) particles found at depth in the Guadiana acidic pit lake (Huelva, Spain); schwertmannite (Schw) particles with hedgehog morphology are also observed coexisting with the hydrobasaluminite. (b) typical XRD patterns of hydrobasaluminites formed by titration in the laboratory (ST-3 and ST-4) and naturally formed in the acidic pit lake of Guadiana (HER55). Reprinted from Sánchez-España et al., 2011 and Sánchez-España et al., 2016b, with permission.

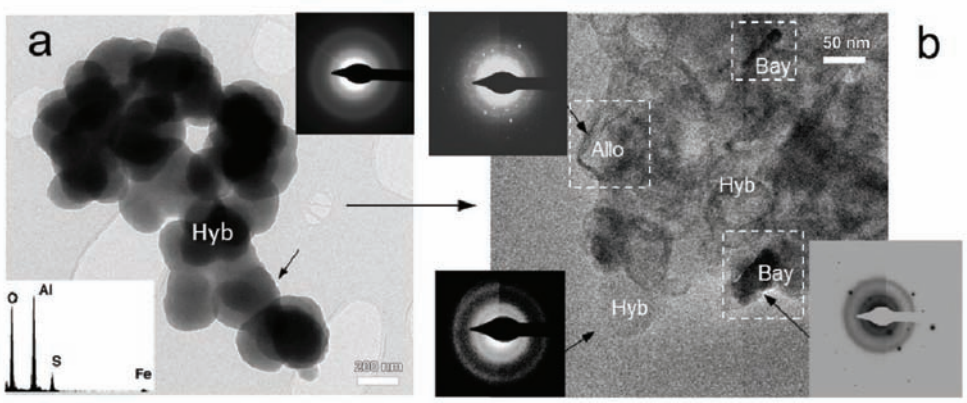

Fig. 4. aTEM images and associated EDS and SAED patterns of aluminum particles found in deep anoxic waters of the Guadiana acidic pit lake: (a) hydrobasaluminite (Hyb) cluster made of nanometric particles which range from subrounded to slightly faceted; (b) nanometric crystals of bayerite (Bay) and allophane (Allo) embedded in amorphous hydrobasluminite matrix (Hyb). Reprinted from Sánchez-España et al., (2016b), with permission.

hydrobasaluminite globules, which has been interpreted as diagnostic of recrystallization and mineral replacement *(Fig. 4b; Sánchez-España et al., 2016b).*

5. Direct crystallization of Fe-Al sulfates

In the previous section, the formation of crystalline (well-ordered) minerals was indirect and resulting from recrystallization of less table precursor phases (i.e., jarosite from schwertmannite, bayerite from hydrobasaluminite; *Figs. 2 and 4b).* However, crystals of jarosite and its related Al counterpart (alunite) can also form directly from solution under certain geochemical and physical (hydrological) conditions *(Sánchez-España et al., 2016a).* Furthermore, because the molar concentrations of Fe(III) and Al in the acidic solutions is often comparable, and as far as the pH range of these waters falls within the stability field for both sulfate minerals, these two pure end-members are rarely seen in nature, and the most common case is to find intermediate members of the jarosite-alunite solid solution *(Alpers et al., 1989; Dutrizac & Jambor, 2000; Sánchez-España et al., 2016a).*

The geochemistry of certain acidic pit lakes favors the precipitation of well-developed crystals of jarosite and alunite, and the low turbulent hydrological conditions of these water bodies allow nucleation and further crystalline growth. The combination of conventional SEM and TEM with high resolution TEM (HRTEM), cryo-TEM, and scanning transmission electron microscopy (STEM) has provided definitive evidence for the simultaneous formation of these two phases *(Fig. 5c).* Moreover, slight fluctuations of the pH conditions in the parent fluid during crystal growth may lead to zoned crystals which record these chemical variations and which can be used to deduce the recent geochemical evolution of these waters *(Figs. 5-6).*

These zoned crystal growths reflect different stages in the crystal formation in which Al atoms or Fe atoms are preferentially incorporated into the crystal lattice as a response to subtle chemical variations. The examples shown in *Figs. 5c and 6* were interpreted to result from a nucleation and early alunite crystal growth phase at pH~3.3, followed by later jarosite crystallization at pH 2.2-2.3 *(Sánchez-España et al., 2016a).* Such difference of around 1 pH unit is important enough to preclude the hydrolysis of Al^{3+} atoms (pK1 Al^{3+}~5.0) and thus their incorporation into the sulfate crystal, while the lower pH value still allows a significant hydrolysis and precipitation of Fe^{3+} (pK1 Fe^{3+}~2.2). Such chemical fluctuations are typical in acidic mine waters as a response to seasonal climatic changes, so that these zoned sulfate crystals may be more common than it has been previously considered.

Depósito legal: CA-602-2004 / ISSN: 1698-5478

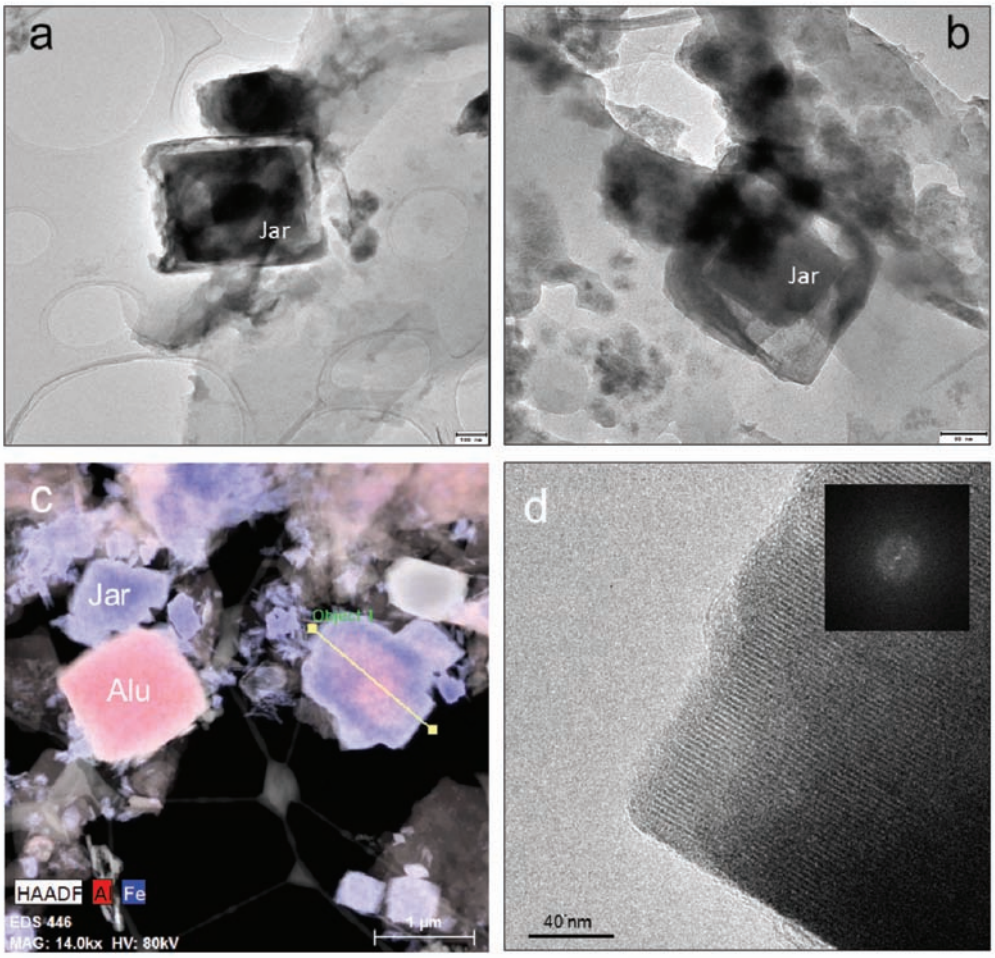

Fig. 5. TEM images of jarosite (Jar) and alunite (Alu) crystals found in San Telmo acidic pit lake: (a-b) zoned crystals of jarosite (scale bar is 100 and 80 nm, respectively); (c) STEM image and elemental mapping of jarosite and alunite end-members coexisting with a zoned crystal having an alunite core surrounded by a jarosite rim (Al shown in red, ferric iron shown in blue); (d) detail of crystalline planes in alunite crystal obtained by HRTEM. Modified from Sánchez-España et al., (2016a), with permission.

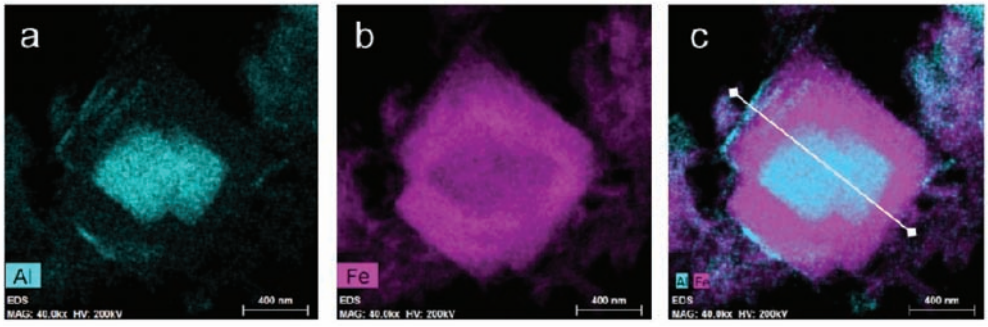

Fig. 6. STEM element mapping showing the Al (blue) and iron (pink) distribution in a zoned crystal precipitated in the water column of San Telmo pit lake (pH 2.2-3.3). Modified from Sánchez-España et al., (2016a), with permission.

Sometimes the crystallization process results in hopper crystals with fully developed edges and empty interiors *(Fig. 7)*. This particular crystal formation usually takes place when the crystal grows so rapidly that there is not sufficient time (or material) to fill in the gaps. Under such conditions, electrical attraction is higher along the edges of the crystal, and this causes faster growth at the edges than near the face centers.

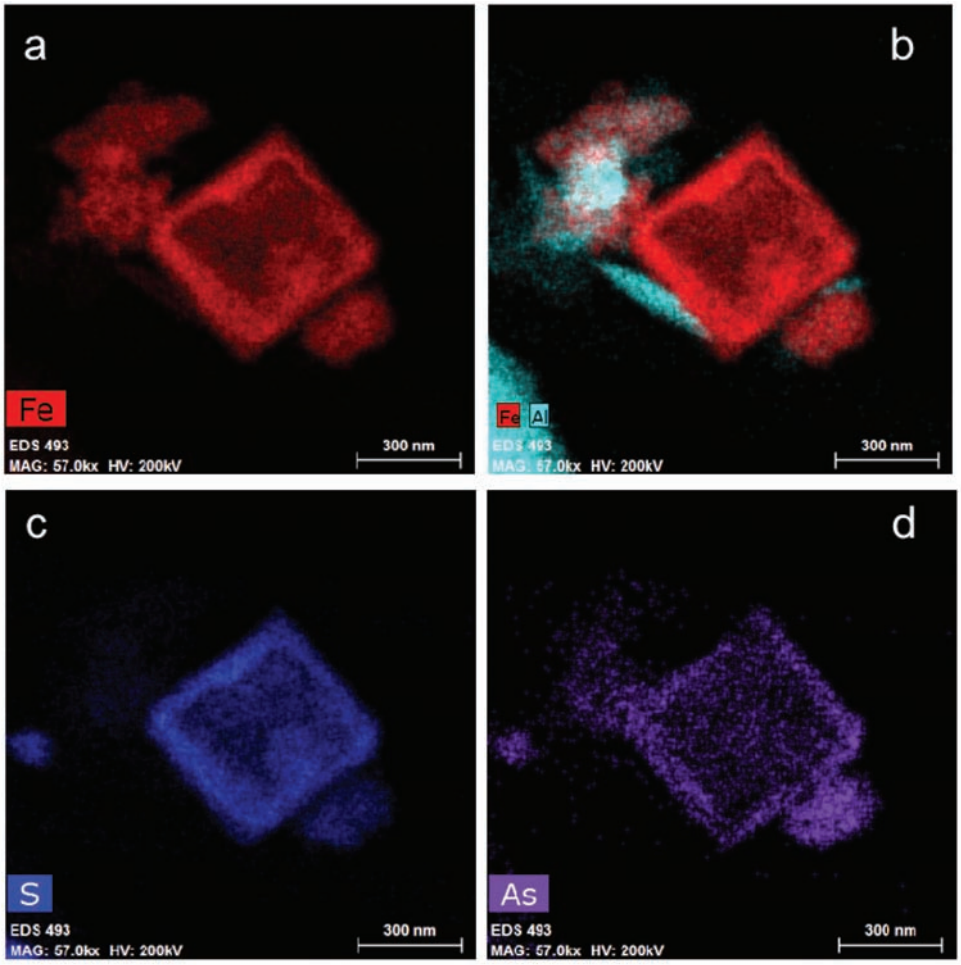

Fig. 7. STEM element mapping showing the distribution of Fe, S and As in a hopper crystal of jarosite formed in San Telmo pit lake. Reprinted from Sánchez-España et al., (2016a), with permission.

6. Metal sulfides formed in reducing and anoxic environments

Bacterial sulfate reduction can also take place at low pH *(Koschorreck, 2008)*. The presence of sulfate-reducing bacteria (SRB, acidophilic or acid-tolerant) in sub-surface environments of acidic waters, under anoxic and highly reducing conditions, can lead to the production of hydrogen sulfide (H_2S) through the reaction:

$$2CH_2O + SO_4^{2-} + 2H^+ \xrightarrow{SRB} 2\,CO_2 + 2\,H_2O + H_2S \qquad (9)$$

where CH_2O represents organic matter .

This biogenic H_2S may then react with metals (e.g., Cu, Cd, Pb, Zn, Fe) or metalloids (e.g., As) to form different sulfide minerals, according to reactions (10-11):

$$H_2S \overset{K_1}{\leftrightarrow} HS^- + H^+ \qquad (10)$$

$$Me^{2+} + HS^- \leftrightarrow MeS\downarrow + H^+ \qquad (11)$$

where Me^{2+} represents a divalent metal cation such as Cu^{2+}, Zn^{2+}, Pb^{2+}, Cd^{2+} or Fe^{2+} *(Lewis, 2010)*.

In a system where different dissolved metals are present, as is the case of most AMD environments, different sulfide minerals may precipitate according to their respective solubilities. Sulfide minerals increase in solubility from CuS (covellite-like, the less soluble) to FeS (mackinawite-like, the most soluble), and as pH increases, a natural sequence of sulfide precipitation in different stages can be observed with the order usually being: CuS > CdS > PbS > As2S3 > NiS > ZnS > FeS *(Diez-Ercilla et al., 2014)*.

In a narrow layer situated immediately below the redoxcline at 11 m depth into the water column of the acidic pit lake of Cueva de la Mora (Huelva, Spain), *Diez-Ercilla et al., (2014)* found different metal sulfides resulting from the sequence of reactions (9-11). The presence and metabolic activity of SRB in this layer (*Wendt-Phottoff et al., 2012; Falagán et al., 2014*) produces H_2S which immediately reacts with dissolved Cu, As or Zn and precipitate at pH between 3.0 and 4.0. Careful examination by electron micros-

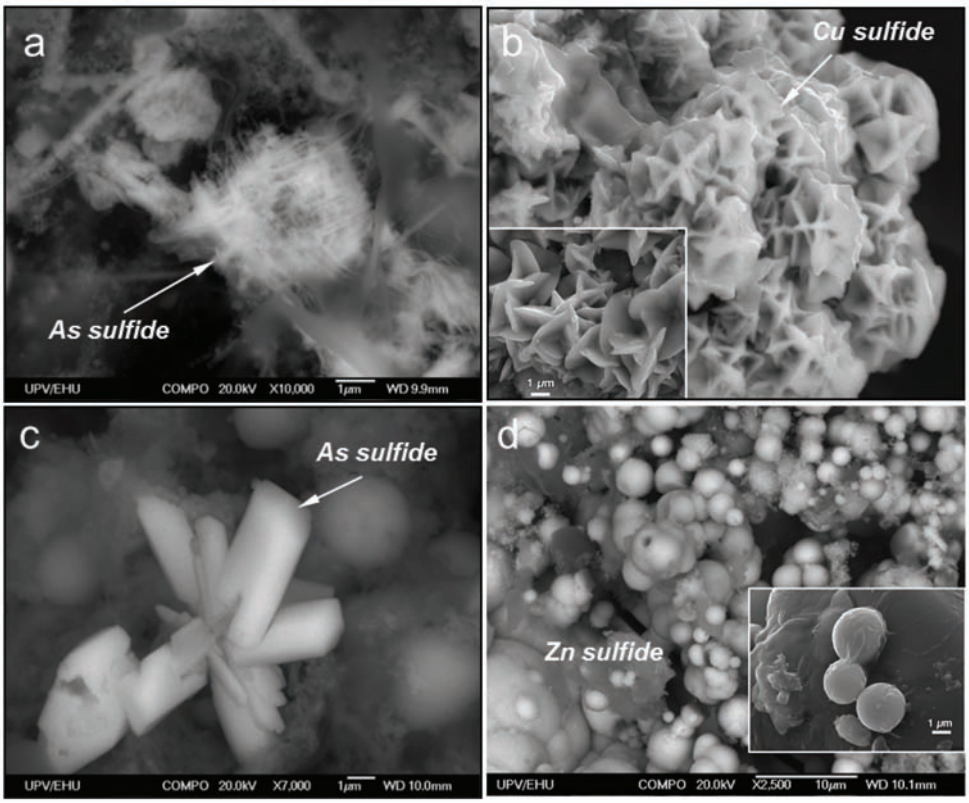

Fig. 8. SEM images of different sulfide minerals found at depth between 11 and 18 m in Cueva de la Mora acidic pit lake: (a) Aggregate with acicular crystals of As sulfide; (b) rosette-like platty crystals of natural Cu sulfide (covellite) – the inset shows a morphologically similar covellite growth obtained in the laboratory; (c) euhedral (prismatic) crystals of As sulfide; (d) spherical particles of amorphous Zn sulfide (likely wurtzite); the inset shows a detail of wurtzite particles analysed by EDS. Modified from Diez-Ercilla et al., (2014).

copy has revealed that these sulfides exhibit highly contrasting crystallinity and morphology, and it is common to observe nearly amorphous, pseudo-spherical particles (e.g., ZnS) coexisting with well-defined crystals (e.g., CuS, covellite; As_2S_3, orpiment) (Fig. 8). Depending on the mineral, crystal habits may comprise whiskers, laths, rods, and also amorphous gel-like aggregates.

Arsenic sulfides show different morphologies, including web- and wire-like aggregates *(Fig. 8a)*, fine granular, and well-formed, prismatic crystals in micrometric clusters *(Fig. 8c)*. The S/As molar ratios, frequently close to S/As=1.3, are usually diagnostic of orpiment stoichiometry (As_2S_3). Amorphous As_2S_3 and orpiment are known to precipitate mainly at low pH and low sulfide concentration .

In contrast to the arsenic sulfides, zinc sulfides have been only identified as spherical ZnS particles *(Fig. 8d)*. This spherulitic morphology is common in fine-grained sphalerite *(Labrenz et al., 2000)* and has been also found in sulfidic acid environments *(e.g.,Church et al., 2007).*

Cupper sulfide precipitates have been also obtained in the laboratory by addition of Cu^{2+} (as $CuSO_4$) to solutions containing H_2S *(Diez-Ercilla et al., 2014)*. These Cu sulfides showed tabular growth with rosette-like aggregates *(Fig. 8b)*. This crystalline morphology has been also occasionally observed in natural samples *(Fig. 8b-inset)*. The obtained S/Cu molar ratios of these crystals ($\simeq$1), and electron diffraction patterns obtained by TEM *(Fig. 9c)* indicate that covellite is the most common Cu sulfide. This mineral can directly precipitate out of solution or, alternatively, it may also form by aging of primitive copper sulfide precursor *(Pattrick et al., 1997; Luther et al., 2002)*. The textural and microstructural features of covellite crystals, often surrounded by exopolymeric substances (EPS) excreted by the bacteria, and also in

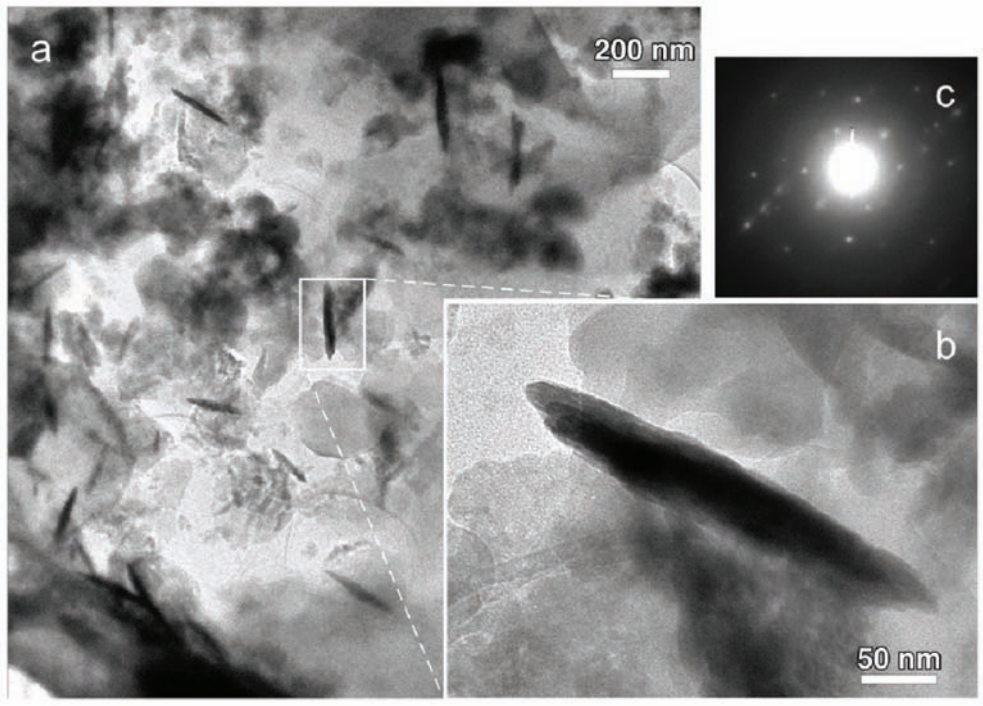

Fig. 9. (a) TEM picture of covellite crystals found at depths of 32 m in Cueva de la Mora acidic pit lake (pH 4.0-4.5); (b) Detail of (a) showing the elongated habit, nanometric width and sub-micron length of a covellite crystal embedded in amorphous matrix; (c) SAED pattern showing brilliant spots diagnostic of major crystalline planes of crystal in (b). Reprinted from Diez-Ercilla et al., (2014), with permission.

Depósito legal: CA-602-2004 / ISSN: 1698-5478

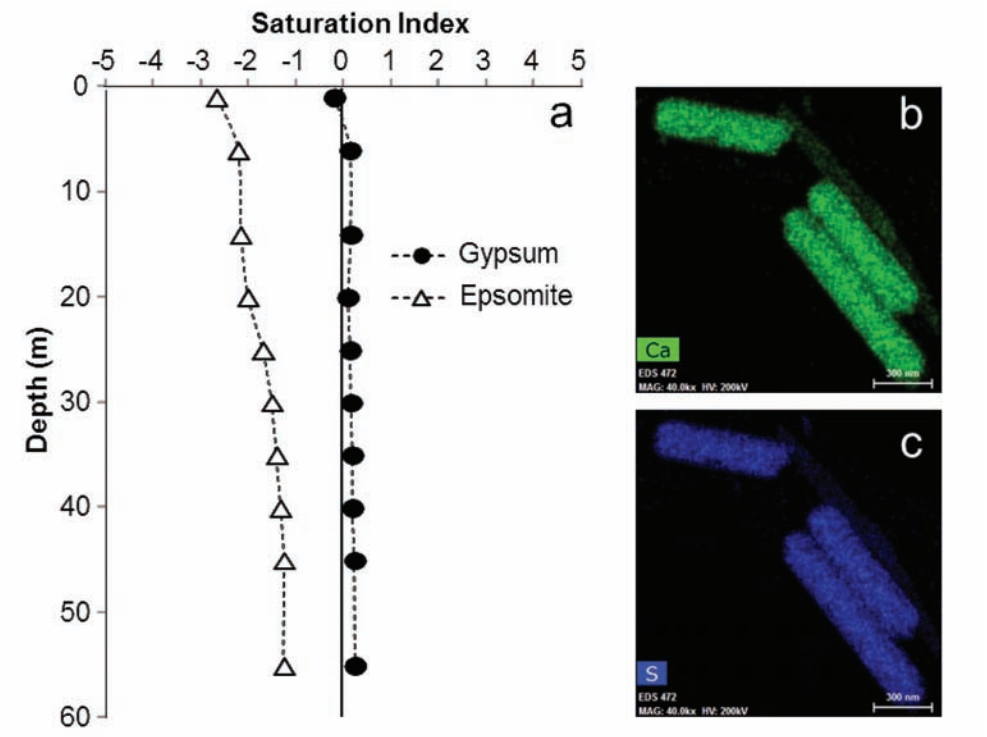

Fig. 10. (a) Vertical evolution of the saturation index (SI, defined as SI=Log[IAP/Ksp]) of gypsum and epsomite, as a function of depth, in the Guadiana acidic pit lake (pH 3.0-4.2); (b-c) False-colour element mapping (obtained by STEM/EDS) showing Ca and S distribution in submicron-sized gypsum crystals naturally formed in the water column of this lake (30-40 m). Modified from Sánchez-España et al., (2014).

close association with amorphous gels of similar composition (CuS) *(Fig. 9)*, suggest that the latter mechanism (i.e., indirect crystallization by crystalline re-arrangement of amorphous precursors) may be the most frequent pathway of covellite crystal formation in these acidic environments.

7. Precipitation of gypsum crystals

Another classical example of crystal formation in acidic solutions is that of gypsum ($CaSO_4 \bullet 2H_2O$). In acid-sulfate solutions, Mg is highly soluble and tends to be conservative (with the exception of evaporative pools), while Ca is less soluble and its aqueous concentration is normally controlled by gypsum solubility *(Nordstrom, 2008)*. The precipitation of gypsum is thus the most important control of Ca concentration in acidic waters. This is often confirmed by geochemical calculations which show gypsum solubility equilibrium and under-saturation for Mg-sulfate species (exemplified by epsomite). A good example of this is the acidic pit lake of Guadiana (Herrerías Mine, Huelva), where gypsum has been observed to form in the water column as a result of solubility saturation *(Fig. 10)*. The plateau observed in *Fig. 10a* results from solubility equilibrium of Ca, and the maximum concentration of this element (up to 600 mg/L Ca) roughly equals the theoretical gypsum solubility limit at the sulfate concentrations found in the lake (5-25 g/L SO_4). Gypsum crystals have been frequently found in the water column of this lake, with idiomorphic (tabular) habit and submicron size *(Fig. 10b-c)*.

Gypsum crystals can also form spontaneously in running acidic waters (e.g., mine effluents, AMD-impacted streams) and in treatment plants where base (often lime) addition to increase the pH of inflowing waters provokes gypsum solubility saturation. In these cases, gypsum is often found as well-

developed tabular crystals, although the length, diameter and habit of these crystals may differ depending on kinetic factors (chiefly, precipitation rate, which in turn depends on neutralization rate) *(Fig. 11)*. Gypsum crystals found in different AMD environments can be as small as 500x100 nm *(Fig. 10b-c)* or as large as mm- to cm-scale *(Fig. 11)*. Atomic substitution of Ca^{2+} for other divalent cations is not frequent, and gypsum crystals are often of high purity despite the metal-rich nature of the precipitating solutions.

If occurring during a sufficiently long time period, the precipitation of gypsum crystals in a given acidic system may remove a substantial amount of calcium from solution even at relatively low pH (e.g., 4.5-5.0), in contrast to other cations like Mg^{2+}, which require much higher pH values (usually above 9.0) to precipitate as an hydroxide or hydroxyl-carbonate *(Sánchez-España & Yusta, 2015)*.

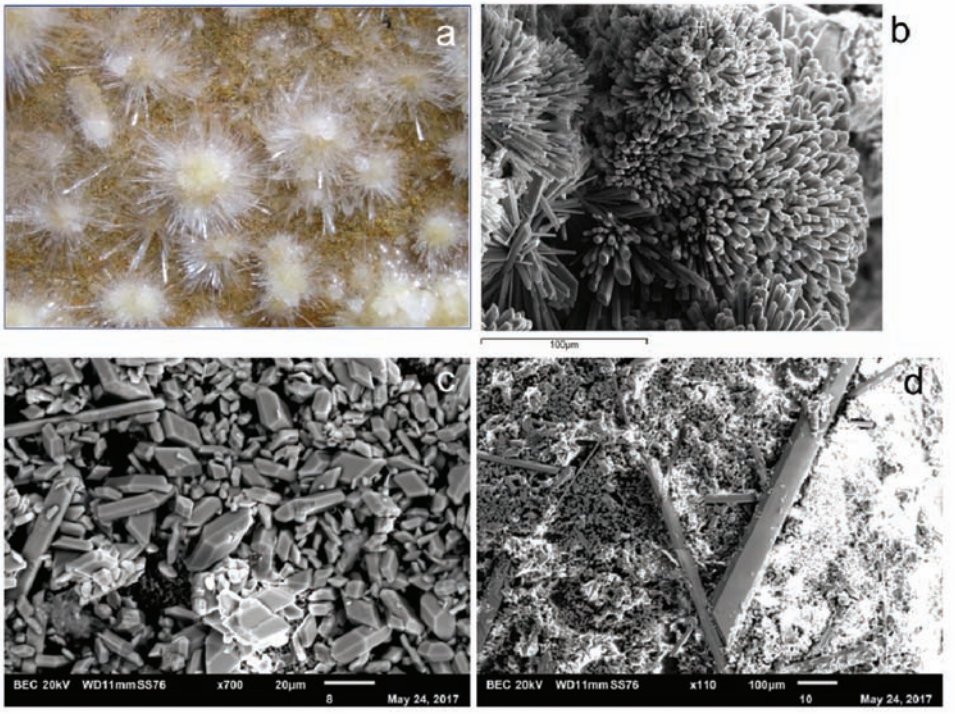

Fig. 11. Different examples of gypsum crystals formed in acidic mine waters: (a) Acicular gypsum crystals growing upwards from a streambed of an acidic mine effluent (field of view~5 cm); (b) Rosette-like growth composed of columnar crystals of gypsum formed in the Tintillo acidic river; (c-d) prismatic crystals formed by neutralization of acidic solutions in the laboratory; smaller crystals of 10-20 mm length precipitated directly in the flasks, while the mm-scale crystals in (d) formed later during filtering and drying. (b) taken from Sánchez-España et al., (2007b).

8. Formation of melanterite and rozenite crystals in evaporative, extremely acidic brines

The formation of efflorescent sulfates is typical in AMD waters and is especially abundant during spring and summer. The mineralogy of these soluble sulfates is closely associated with their spatial distribution and the pH of the brines from which these salts are precipitated *(Nordstrom & Alpers, 1999b; Jambor et al., 2000; Nordstrom et al., 2000; Buckby et al., 2003; Sánchez-España et al., 2005; Velasco et al., 2005)*. Thus, Fe(II)-sulfates like melanterite, rozenite or szomolnokite are dominant in isolated and highly concentrated pools near the pyrite sources, under conditions typical of green, ferrous AMD with very low pH. On the other hand, mixed Fe(II)-Fe(III), and/or Fe(III)-Al sulfates like copiapite, coquimbite or halotrichite, are

Depósito legal: CA-602-2004 / ISSN: 1698-5478

common in the margins of rivers impacted by AMD, where iron has been partially oxidized and the pH is slightly higher (typically between 1.5 and 3). These sulfates have been observed to follow a paragenetic sequence with melanterite > rozenite > szomolnokite > copiapite > coquimbite > rhomboclase > halotrichite *(Nordstrom & Alpers, 1999a,b; Jambor et al., 2000; Buckby et al., 2003; Velasco et al., 2005)*. Chemical analyses of mixtures of these sulfates have revealed very high metal contents (e.g., average values of 2,800 ppm Cu and 9,000 ppm Zn, with Zn values eventually reaching percent units; *Sánchez-España et al., 2005)*, so that the precipitation-redissolution cycle of these salts is of high environmental relevance.

When acidic water stands in contact with pyrite during a sufficiently long period of time (long residence time and low water flow favouring mineral/water interaction), the combination of several chemical and physical processes can lead to the formation of extremely acidic waters with abnormally high concentrations of sulfate, ferrous iron and other metals *(Nordstrom & Alpers, 1999b; Nordstrom et al., 2000; Alpers et al., 2003; Sánchez-España et al., 2008).* The continuous dissolution of pyrite, coupled with the oxidation of Fe(II) to Fe(III) and the further oxidation of pyrite by Fe(III) within a relatively small water volume, provokes a continuous *"iron wheel"* which continuously solubilizes material and increases dramatically the solute concentration. If this process takes place in an arid or semi-arid region, where high ambient temperatures enhance pyrite dissolution and evaporation, the result may be an acid water with pH close to zero and sulfate concentrations in the order of hundreds of grams per litre. Under these conditions, the salinity and ionic strength is so high (e.g., several times that of seawater) that the conventional equations and activity coefficients used in common geochemical modelling software cannot be applied, since the electrostatic attraction and interaction between atoms in these brines is much more important than in dilute solutions, and deviations from the ideal behaviour can be very high *(Nordstrom et al., 2000; Sánchez-España & Diez-Ercilla, 2008; Sánchez-España et al., 2008)*. In the most extreme case known to date, *Nordstrom et al., (2000)* reported even negative pH values (due to H^+ activity being higher than 1.0), sulfate concentration of 0.76 kg/L and dissolved iron concentration of 0.11 kg/L in waters found in Iron Mountain mine, California. In Spain, *Sánchez-España et al., (2008)* also reported the occurrence of green pools of extremely acidic water (pH 0.6) with similarly extreme concentrations of dissolved sulfate (134 g/L SO_4) and iron (61 g/L Fe_t) in San Telmo mine. Despites its low pH, however, this acidic liquour was close to saturation with respect to melanterite, and well-formed crystals were observed to precipitate directly from solution *(Fig. 12a-b)*. The formation of these crystals occurs when the Fe^{2+} and SO_4^{2-} concentrations reach the solubility product constant for melanterite, and reaction (12) takes places until chemical equilibrium is attained:

$$Fe^{2+} + SO_4^{2-} + 7H_2O \rightarrow FeSO_4 \cdot 7H_2O_{(s)} \quad (12)$$

The formation of crystals of melanterite and its associated mineral rozenite ($FeSO_4 \cdot 4H_2O$) has been also observed in the margins of low-flow acidic streams with high Fe(II) concentrations (thus, close to the mining areas; *Fig. 12c*), and in porewaters in pyritic soils or sludges *(Fig. 12d)*. The crystallization process in these environments usually takes place under hydrologically and kinetically favourable conditions (i.e., low flow or standing water, slow precipitation kinetics) which facilitate crystal growth. Thus, it is common to observe cm-scale macroscopic crystals showing well-developed concentric or parallel growths (*Fig. 12b,d*).

As discussed in a previous section, in addition of Fe^{2+}, the acidic mine waters usually have very high concentrations of other divalent metal cations, such as Cu^{2+} or Zn^{2+}. The size and atomic radius of these two cations is not very different from that of Fe^{2+}, so that their incorporation into the melanterite crystal lattice is structurally possible, and Cu-rich and Zn-rich melanterites are frequent in these environments. As an example, some melanterite crystals shown in *Fig. 12* displayed trace metal concentrations as high as 1.3 %wt. Zn and 0.7 %wt. Cu

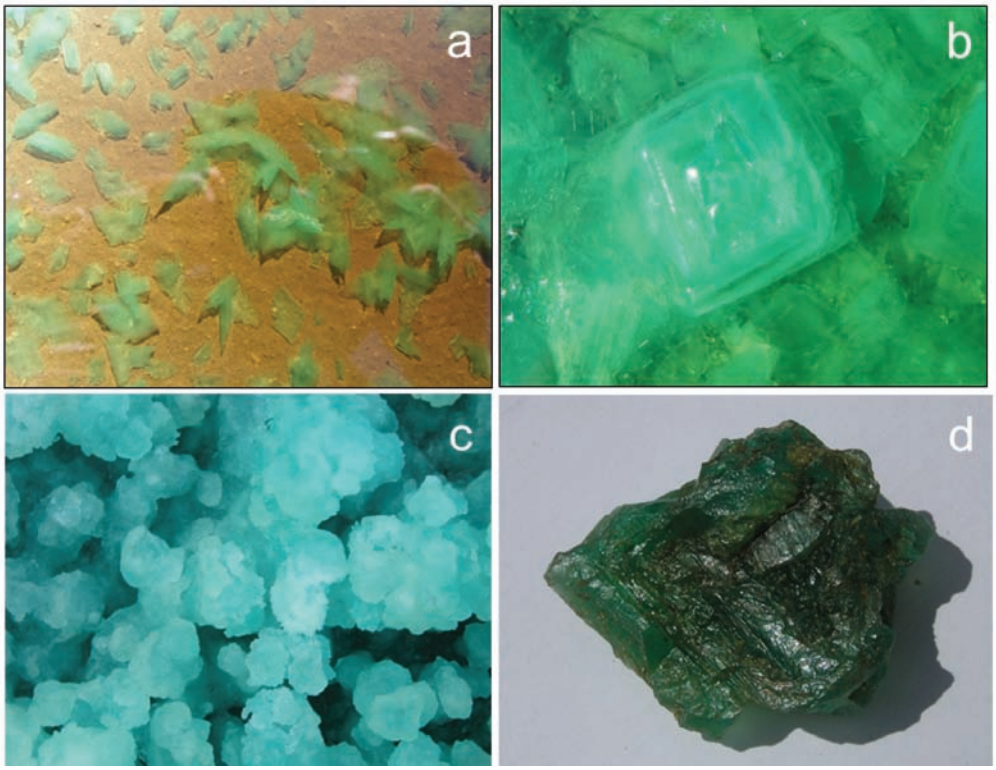

Fig. 12. (a-b) Emerald-green melanterite crystals formed in extremely acidic (pH 0.6) ferrous sulfate brine solutions in contact with fin-grained pyritic sludge in San Telmo mine (Huelva). Photo (a) courtesy of Dr. Francisco Velasco (UPV/EHU), (a-b) from Sánchez-España et al., (2008); (c) Cu-rich, blue-coloured melanterite crystals forming an efflorescence in the margins of an evaporating acidic stream in San Telmo mine; (d) Large crystal of rozenite formed in pore waters of a soil with pyritic sludge in Tharsis mine (Huelva). The fields of view are 10 cm (a), 2 cm (b), 5 cm (c), and 8 cm (d).

(Sánchez-España et al., 2008; Sánchez-España & Diez-Ercilla, 2008).

The theoretical simulation of melanterite crystallization from these acidic brines through geochemical modelling must be accomplished by using models for concentrated solutions, as discussed before. The Pitzer specific-ion-interaction theory of activity correction for calculation of activity coefficients in brines and electrolyte solutions *(Pitzer, 1986; Plummer et al., 1988)* has been shown to work well in these aqueous systems. An example of melanterite precipitation model for the specific case of the San Telmo acidic brine was presented by *Sánchez-España &Diez-Ercilla (2008) (Fig. 13)*. This model compared the solubility of melanterite (as defined by its saturation index) as calculated with the conventional Davis equation for dilute solutions with that resulting of applying the Pitzer theory with MacInnes convention. The plot shown in *Fig. 13a* shows that, as expected, the Davis equation cannot predict satisfactorily the precipitation of melanterite crystals at the chemical conditions prevailing in the parent solution, whereas the Pitzer/MacInnes approach accurately establishes the beginning of melanterite crystallization at a sulfate concentration which roughly corresponds to that measured in the acidic liquour at the time of sampling. The application of the Pitzer approach also predicted cycles of melanterite crystallization followed by crystal re-dissolution as a response to natural diurnal temperature oscillations, with colder temperatures prevailing at night favouring crystallization, and hotter day-time temperatures favouring crystal re-dissolution *(Fig. 13b)*.

Depósito legal: CA-602-2004 / ISSN: 1698-5478

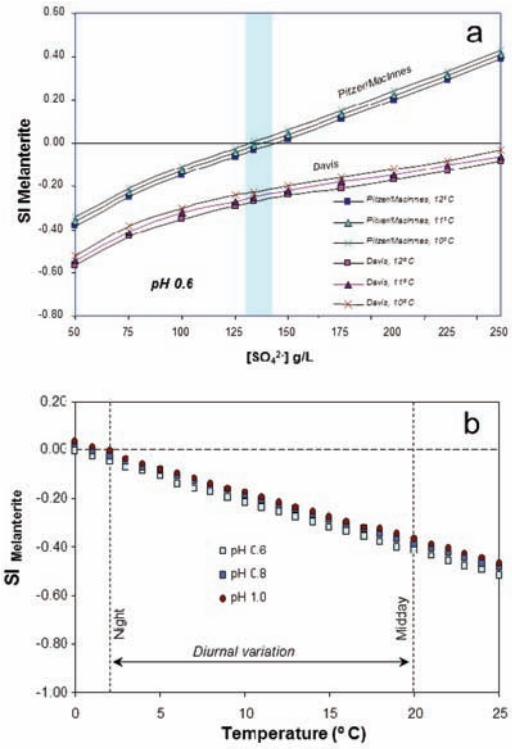

Fig. 13. Variation of the saturation index (SI) with respect to melanterite solubility as a function of sulfate concentration (a) and temperature (b) in an extremely acidic (pH 0.6) and ultra-concentrated liquor emanating from a pyrite pile in San Telmo mine (Huelva). In (a), the SI calculated for different temperatures and using two different approaches (Davis vs. Pitzer) are shown for comparison. The blue area indicates the range of sulfate concentration measured in this brine. In (b), the temperature-dependence of SImelanterite is shown for different pH values and using the Pitzer/MacInnes approach. The melanterite crystals formed in this environment are shown in Fig. 12(a-b). Modified from Sánchez-España et al., (2008) & Sánchez-España and Diez-Ercilla (2008).

9. Conclusions

The mineralogical composition, particle size and degree of crystallinity of the solids formed in low pH systems are strongly influenced by the chemical and physical factors which characterize this particular type of waters. Chemically, the singular chemistry of the parent acidic solutions usually includes highly concentrated, sulfate-rich waters with presence of many dissolved metals. Physically, the conditions prevailing in the crystallization media are highly variable and may range from very fast to slow precipitation kinetics, from strong oversaturation to near solubility equilibrium, or from high to low density of nucleation centres. In coherence with these chemical and physical conditions, the most common mineral groups formed in acidic waters (e.g., acid mine waters, acid rock drainage) are usually metal sulfates, oxy-hydroxysulfates and sulfides, which expand largely in size and crystalline order. Particle or crystal sizes normally range from diameters < 100 nm (which are within the range of natural nano-particles and thus make them behave as colloids in the solutions) to large crystals of macroscopic (mm- to cm-) scale. The former sizes are usually associated with nearly amorphous or short-range ordered oxyhydroxysulfates (e.g., schwertmannite, hydrobasluminite) formed in supersaturated solutions with relatively fast precipitaton kinetics, but can also include nano- to sub-micron crystals precipitated directly from solution (e.g., gypsum) or by transformation of metastable precursors (e.g., bayerite or allophane from hydrobasaluminite recrystallization). The latter sizes are more often found in near-equilibrium environments where the slow crystallization kinetics allow formation of large and well-developed crystals. A classical example is the formation of melanterite or rozenite in super-concentrated acidic brines formed by evaporative processes near the oxidising-pyrite sources.

10. Acknowledgements

I would like to thank Dr Amalia Jimenez (Oviedo University, Department of Geology) and the Spanish Society of Mineralogy (SEM) for their kind invitation to present this talk at the “Crystallization under extreme conditions” workshop (Oviedo, July 4th, 2017). I also thank Dr Iñaki Yusta (Basque Country University, Department of Mineralogy) with whom I have shared so many hours of SEM and TEM work, as well as many vibrant discussions, during the last years. Pictures and information provided in this communication have been obtained during different research projects funded the Spanish Ministry of Economy (*Secretaría de Estado de Investigación, Desarrollo e Innovación) through the Plan Estatal de Investigación Científica y Técnica y de Innovación* (REN2003-09590-C-04-04, CGL2009-07090, CGL2016-74984-R), and the Spanish Ministry of Culture, Education and Sports (PRX14/00087).

References

Acero, P., Ayora, C., Torrentó, C. & Nieto, J.M. (2006) The behaviour of trace elements during schwertmannite precipitation and subsequent transformation into goethite and jarosite. Geochim. Cosmochim. Acta, 70, 4130-4139.

Alpers, C.N., Nordstrom, D.K. & Ball, J.W. (1989) Solubility of jarosite solid solutions precipitated from acid mine waters, iron Mountain, califronia, USA. Sci. Géol. Bull., 42-4, 281-298.

Alpers, C.N., Nordstrom, D.K. & Spitzley J. (2003) Extreme acid mine drainage from a pyritic massive sulphide deposit: The Iron Mountain end-member. (In J.L. Jambor, D.W. Blowes, & A.I.M. Ritchie (Eds.) Environmental Aspects of Mine wastes, Mineralogical Association of Canada, Short Course Series Volume 31 (R Raeside, ed.), pp. 407-430, Vancouver, British Columbia.

Ashcroft, N.W. & Mermin, N.D. (1976) Solid state physics. Brooks/Cole, 848 p.

Battaglia-Brunet, F., Crouzet, C., Burnol, A., Coulon, S., Morin, D. & Joulian, C. (2012) Precipitation of arsenic sulphide from acidic water in a fixed-film bioreactor. Water Res. 46, 3923–33.

Bigham, J.M., Carlson, L. & Murad, E. (1994) Schwertmannite, a new iron oxyhydroxysulfate from Pyhäsalmi, Finland, and other localities. Mineral. Mag., 58, 641-648.

Bigham, J.M., Schwertmann, U., Traina, S.J., Winland, R.L. & Wolf, M. (1996) Schwertmannite and the chemical modeling of iron in acid sulfate waters. Geochim. Cosmochim. Acta, 60, 2111-2121.

Bigham, J.M., Nordstrom, D.K. (2000) Iron and Aluminum Hydroxysulfates from Acid Sulfate Waters. In Sulfate Minerals: Crystallography, Geochemistry, and Environmental Significance (Alpers, C.N., Jambor, J.L., Nordstrom, D.K. (Eds.). Reviews in Mineralogy & Geochemistry, 40, 351-403.

Buckby, T., Black, S., Coleman, M.L. & Hodson, M.E. (2003) Fe-sulphate-rich evaporative mineral precipitates from the Río Tinto, southwest Spain. Mineral. Mag., 67, 263-278.

Church, C.D., Wilkin, R.T., Alpers, C.N., Rye, R.O. & McCleskey, R.B. (2007) Microbial sulfate reduction and metal attenuation in pH 4 acid mine water. Geochem. Trans. 8, 10-24.

Diez-Ercilla, M., Sánchez-España, J., Yusta, I., Wendt-Phottoff, K. & Koschorreck, M. (2014) Formation of biogenic sulphides in the water column of an acidic pit lake: Biogeochemical controls and effects on trace metal dynamics. Biogeochemistry 121, 519-536.

Dutrizac, J.E. & Jambor, J.L. (2000) Jarosites and their application in hydrometallurgy. In Sulfate Minerals: Crystallography, Geochemistry, and Environmental Significance (Alpers, C.N., Jambor, J.L., Nordstrom, D.K., Eds.). Reviews in Miner. & Geochem., 40, 405-452.

Falagán, C., Sánchez-España, J. & Johnson, B. (2014) New insights into the biogeochemistry of extremely acidic environments revealed by a combined cultivation-based and culture-independent study of two stratified pit lakes. FEMS Microbiology Ecology 87(1), 231-243.

Ferris, F.G., Hallbeck, L., Kennedy, C.B. & Pedersen, K. (2004) Geochemistry of acidic Rio Tinto headwaters and role of bacteria in solid phase metal partitioning. Chemical Geology, 212, 291-300.

Frau, F. (2000) The formation-dissolutionprecipitation cycle of melanterite at the abandoned pyrite mine of Genna Luas in Sardinia, Italy: environmental implications. Mineral Mag, 64, 995-1006.

Furrer, G., Phillips, B.L., Ulrich, K-U, Pöthig, R. & Casey, W. (2002) The origin of aluminum flocs in polluted streams. Science 297, 2245-2247.

Garrels, R.M. & Thompson, M.E. (1960) Oxidation of pyrite by iron sulfate solutions. Am J Sci, 258A, 57-67.

Goetz, A.J., Ziegler, A., Gaebel, J., Wiacek, C., Schlömann, M. & Schmahl, W.E. (2010) Structural variations in biogenic and synthetic schwertmannite. Macla 13, 118.

Hochella M.F. (2008) Nanogeoscience: From origins to cutting-edge applications. Elements 4, 373-379.

Jambor, J.L., Nordstrom, D.K. & Alpers, C.N. (2000) Metal-sulfate salts from sulfide mineral oxidation. In Sulfate Minerals. Alpers, C.N., Jambor, J.L. & Nordstrom, D.K (eds), Reviews in Mineralogy and Geochemistry, 40-6, 303-350.

Jönsson, J., Persson, P., Sjöberg, S. & Lövgren, L. (2005) Schwertmannite precipitated from acid mine drainage: phase transformation, sulfate release and

surface properties. Appl. Geochem., 20, 179-191.

Kawano, M. & Tomita, K. (2001) Geochemical modeling of bacterially induced mineralization of schwertmannite and jarosite in sulfuric acid spring water. Am. Mineral., 86, 1156-1165.

Kim, J.J. & Kim, S.J. (2003) Environmental, mineralogical, and genetic characterization of ochreous and white precipitates from acid mine drainages in Taebaeg, Korea. Environ. Sci. Technol., 37, 2120-2126.

Koschorreck, M. (2008) Microbial sulfate reduction at a low pH. FEMS Microbiol. Ecol. 64, 329–42.

Labrenz, M., Druschel, G.K., Thomsen-Ebel, T., Gilbert, B., Welch, S.A., Kemner, K.M., Logan, G.A., Summons, R.E., De Stasio, G., Bond, P.L., Lai, B., Kelly, S.D. & Banfield, J.F. (2000) Formation of sphalerite (ZnS) deposits in natural biofilms of sulfate-reducing Bacteria. Science 290, 1744–1747.

Lewis, A.E. (2010) Review of metal sulfide precipitation. Hydrometallurgy 104, 222–234.

Luther, G.W., Theberge, S.M., Rozan, T.F., Rickard, D., Rowlands, C.C. & Oldroyd, A. (2002) Aqueous copper sulfide clusters as intermediates during copper sulfide formation. Environ. Sci. Technol. 36, 394–402.

McKibben, M.A. & Barnes, H.L. (1986) Oxidation of pyrite in low temperature acidic solutions – rate laws and surface textures. Geochim Cosmochim Acta, 50, 1509-1520.

Mullin, J.W. (2011) Crystallization, 4th Ed. Butterworth-Heinemann, 600 p.

Nordstrom, D.K. (1982) The effect of sulfate on aluminum concentrations in natural waters: some stability relations in the system Al203-SO3-H20 at 298 K. Geochim. Cosmochim. Acta 46, 681-692.

Nordstrom, D.K. (1985) The rate of ferrous iron oxidation in a stream receiving acid mine effluent. Selected papers in the hydrologic sciences. US Geological Survey Water Supply Paper 113-119.

Nordstrom, D.K. (2008) Questa baseline and pre-mining ground-water quality investigation, 25. Summary of results and baseline and pre-mining ground-water geochemistry, Red River Valley, Taos County, New Mexico, 2001-2005. US Geological Survey Professional Paper 1728, 111 p.

Nordstrom, D.K. & Ball, J.W. (1986) The geochemical behavior of aluminum in acidified surface waters. Science 232, 54-56.

Nordstrom, D.K., & Alpers, C.N. (1999a) Geochemistry of acid mine waters. In: Plumlee, G.S. & Logsdon, M.J. (eds.), The Environmental Geochemistry of Mineral Deposits, Part A. Processes, Techniques, and Health Issues: Society of Economic Geologists, Rev. Econ. Geology 6A, 133-156.

Nordstrom, D.K. & Alpers, C.N. (1999b) Negative pH, efflorescent mineralogy, and consequences for environmental restoration at the Iron Mountain Superfund site, California. Proc. Natl. Acad. Sci., 96, 3455-3462.

Nordstrom, D.K., Ptacek, C.J. & Blowes, D.W. (2000) Negative pH and extremely acidic mine waters from Iron Mountain, California. Environ Sci Technol, 34, 254-258.

Nordstrom, D.K. & Archer, D. (2003) Arsenic thermodynamic data and environmental geochemistry. In Welch, A. & Stollenwerk, K. (Eds.), Arsenic in Ground Water, Kluwer Publisher, pp. 1–26.

Pattrick, R.A.D., Mosselmans, J.F.W., Charnock, J.M., England, K.E.R., Helz, G.R., Garner, C.D. & Vaughan, D.J. (1997) The structure of amorphous copper sulfide precipitates: An X-ray absorption study. Geochim. Cosmochim. Acta 61, 2023–2036.

Pitzer, K.S. (1986) Theoretical considerations of solubility with emphasis on mixed aqueous electrolytes. Pure App Chem, 58-12, 1599-1610

Plummer, L.N., Parkhurst, D.L., Fleming, G.W. & Dunkie, S.A (1988) A computer program incorporating Pitzer's equations for calculation of geochemical reactions in brines. U.S. Geol. Survey, Water-Resources Investigations Report 88-4153, Reston, Virginia.

Postgate, J.R. (1984) The sulfate-reducing bacteria, second. ed. Cambridge University Press, Cambridge, UK.

Regenspurg, S., Brand, A. & Peiffer, S. (2004) Formation and stability of schwertmannite in acidic mining lakes. Geochim. Cosmochim. Acta, 68-6, 1185-1197.

Ritchie, A.I.M. (2003) Oxidation and gas transport in piles of sulphidic material. (In Jambor, J.L. Blowes, D.W. & Ritchie A.I.M., Eds.) Environmental Aspects of Mine wastes, Mineralogical Association of Canada, Short Course Series Volume 31 (R Raeside, ed.), pp. 73-94, Vancouver, British Columbia.)

Sánchez-España, J. (2007) The behavior of iron and alu-

minum in acid mine drainage: Speciation, Mineralogy, and Environmental Significance. In T.M. Letcher (ed.), Thermodynamics, Solubility and Environmental Issues, Elsevier B.V., The Netherlands, pp. 137-149.

Sánchez-España, J. & Yusta, I. (2015) Low-crystallinity products of trace metal precipitation in neutralized pit-lake waters without ferric and aluminous adsorbent: Geochemical modelling and mineralogical analysis. Mineralogical Magazine 79(3), 781-798.

Sánchez-España, J., López-Pamo, E. & Santofimia, E. (2007a) The oxidation of ferrous iron in acidic mine effluents from the Iberian Pyrite Belt (Odiel Basin, Huelva, Spain): Field and laboratory rates. Journal of Geochemical Exploration 92, 120-132.

Sánchez-España J., Santofimia E. & López-Pamo E. (2007b) Iron terraces in acid mine drainage systems: A discussion about the organic and inorganic factors involved in their formation through observations from the Tintillo acidic river (Riotinto mine, Huelva, Spain). Geosphere 3(3), 133-151.

Sánchez-España, J., López Pamo, E., Santofimia, E., Aduvire, O., Reyes, J. & Barettino, D. (2005) Acid Mine Drainage in the Iberian Pyrite Belt (Odiel river watershed, Huelva, SW Spain): Geochemistry, Mineralogy and Environmental Implications. Applied Geochemistry 20-7, 1320-1356.

Sánchez-España, J., López-Pamo, E., Santofimia, E., Reyes, J. & Martín Rubí, J.A. (2006) The removal of dissolved metals by hydroxysulfate precipitates during oxidation and neutralization of acid mine waters, Iberian Pyrite Belt. Aquat Geochem 12, 269-298.

Sánchez-España, J. & Diez Ercilla, M. (2008) Geochemical modelling of concentrated mine waters: A comparison of the Pitzer ion-interaction theory with the ion-association model for the study of melanterite solubility in San Telmo mine (Huelva, Spain). In Stefánsson O. (Ed.), Geochemistry Research Advances, Nova Science Publishers, New York, p. 31-55.

Sánchez-España, J., Diez Ercilla, M., González Toril, E., López-Pamo, E., Santofimia Pastor, E., San Martín-Úriz, P. & Amils, R. (2008) Biogeochemistry of a hyperacidic and ultraconcentrated pyrite leachate in San Telmo (Iberian Pyrite Belt, Spain). Water, Air and Soil Pollution, 194, 243-257.

Sánchez-España J., Yusta I. & Diez M. (2011) Schwertmannite and hydrobasaluminite: A re-evaluation of their solubility and control on the iron and aluminum concentration in acidic pit lakes. Applied Geochemistry 26, 1752-1774.

Sánchez-España, J., Yusta, I. & López, G. A (2012) Schwertmannite to jarosite conversion in the water column of an acidic mine pit lake. Mineral. Mag. 76, 2659–2682.

Sánchez-España, J., Boehrer, B. & Yusta, I. (2014) Extreme carbon dioxide concentration in acidic pit lakes provoked by water/rock interaction. Environ. Sci. Technol. 48(8), 4273–4281.

Sánchez-España, J., Yusta, I., Gray, J. & Burgos, W.D (2016a) Geochemistry of dissolved aluminum at low pH: Extent and significance of Al-Fe(III) coprecipitation below pH 4.0. Geochim Cosmochim Acta, 175, 128-149.

Sánchez-España, J., Yusta, I. & Burgos, W.D. (2016b) The geochemistry of dissolved aluminum at low pH: Hydrobasaluminite formation and interaction with silica, trace metals and microbial cells under anoxic conditions. Chemical Geology 192, 70-96.

Singer, P.C. & Stumm, W. (1970) Acidic mine drainage: the rate-determining step. Science, 167, 1121-1123.

Stoffregen, R.E., Alpers, C.N. & Jambor, J.L. (2000) Alunite-Jarosite crystallography, thermodynamics, and geochronology. In Sulfate Minerals: Crystallography, Geochemistry, and Environmental Significance (Alpers, C.N., Jambor, J.L., Nordstrom, D.K., Eds.). Reviews in Mineralogy & Geochemistry, 40, 453-479.

Stumm, W. & Morgan, J.J. (1996) Aquatic chemistry, 3th ed. John Willey & Sons, New York.

Tavare, N.S. (1995) Industrial crystallization. Plenum Press, New York.

Velasco, F., Alvaro, A., Suarez, S., Herrero, M. & Yusta, I. (2005) Mapping Fe-bearing hydrated sulfate minerals with short wave infrared (SWIR) spectral analysis at San Miguel mine environment, Iberian Pyrite Belt (SW Spain). J. Geochem. Expl., 87-2, 45-72.

Wendt-Potthoff, K., Koschorreck, M., Diez-Ercilla, M. & Sánchez-España, J. (2012) Microbial activity and biogeochemical cycling in a nutrient-rich meromictic acid pit lake. Limnologica - Ecology and Management of Inland Waters 42(3), 175-188.

Yang, C. H. & Qiu, H. (1986) Theory of homogeneous nucleation: A chemical kinetic view. The Journal of Chemical Physics 84, 416